Towards hyperentangled time-bin and polarization superdense teleportation in space

Chapman, Joseph, Miller, Ian, Call, Ian, Oshiro, Leo, Zajdela, Matthias, et al.

Joseph C. Chapman, Ian Miller, Ian Call, Leo Oshiro, Matthias Zajdela, Brooke Polak, Paul G. Kwiat, "Towards hyperentangled time-bin and polarization superdense teleportation in space," Proc. SPIE 11167, Quantum Technologies and Quantum Information Science V, 1116702 (19 September 2019); doi: 10.1117/12.2537081

SPIE.

Event: SPIE Security + Defence, 2019, Strasbourg, France

Towards hyperentangled time-bin and polarization superdense teleportation in space

Joseph C. Chapman[a,b], Ian Miller[c], Ian Call[a,b], Leo Oshiro[a,b], Matthias Zajdela[a,b], Brooke Polak[a,b], and Paul G. Kwiat[a,b]

[a]Illinois Quantum Information Science and Technology Center, University of Illinois at Urbana-Champaign, 1110 W. Green St., Urbana, USA
[b]Dept. of Physics, University of Illinois at Urbana-Champaign, 1110 W. Green St., Urbana, USA
[c]Light Machinery, Inc., 80 Colonnade Road North, Unit #1, Ottawa, Canada

ABSTRACT

Quantum communication networks based on fiber optics are restricted in length since efficient quantum repeaters are not yet available. A free-space channel between a satellite in orbit and Earth can circumvent this problem. We have constructed a system to demonstrate the feasibility of quantum communication between space and earth using photons hyperentangled in their polarization and time-bin degrees of freedom. With this system, we have implemented superdense teleportation (SDT) with a fidelity of 0.94±0.02. To increase the efficiency of SDT, we have developed an active, polarization-independent switch compatible with SDT. We characterized the performance of its switching efficiency. Finally, we have constructed a novel two-level interferometer for time-bin qubit creation and analysis in orbit, and bounded its stability.

Keywords: Quantum communication, hyperentanglement, superdense teleportation, interferometer, optical switch

1. INTRODUCTION

For very long distance transmission of quantum information, free-space channels have higher transmission compared to fiber optic channels due to exponential scaling of absorption per unit length in optical fiber compared to the polynomial scaling from diffraction in free space. It is important to maximize transmission of quantum communication channels because a noiseless quantum amplifier is physically impossible, due to the no-cloning theorem. Atmospheric turbulence and the curvature of the earth limit propagation parallel to the earth's surface to ~ 100 km. Transmitting the quantum signal to/from a satellite in orbit, e.g., the International Space Station (ISS), avoids the exponential loss of fibers and heavy atmospheric turbulence of a ground-to-ground free-space link.[1,2]

We think that a valuable demonstration of space-to-earth optical quantum communication could involve several protocols; here we discuss superdense teleportation (SDT),[3] involving polarization and time-bin hyperentangled photons, due to the relatively low level of required technology development and high utility of the results from such a demonstration. Superdense teleportation is a 3-party protocol. Alice facilitates the communication from Charles to Bob of a state of the form

$$|\Psi\rangle = \frac{1}{\sqrt{N}}(|0\rangle + e^{i\phi_1}|1\rangle + e^{i\phi_2}|2\rangle + ...e^{i\phi_{N-1}}|(N-1)\rangle). \quad (1)$$

Alice first shares with Charles half of an entangled state and distributes to Bob the other half of an entangled state of the form

$$|\Psi\rangle = \frac{1}{\sqrt{N}}(|00\rangle + |11\rangle + |22\rangle + ...|(N-1)(N-1)\rangle). \quad (2)$$

Send correspondence to: jchapmn2@illinois.edu

Quantum Technologies and Quantum Information Science V, edited by Mark T. Gruneisen, Miloslav Dusek, Paul M. Alsing, John G. Rarity, Proc. of SPIE Vol. 11167, 1116702
 · doi: 10.1117/12.2537081

Charles can then locally apply phases ϕ_1, ϕ_2, ...$\phi_{N-1} \in [0, 2\pi)$ to transmit his desired state, after which Alice makes a measurement in a mutually unbiased basis from the one which Charles applied his phases. This projects Bob's photon into one of four states, depending on the outcome of Alice's measurement. After applying the correct unitary gate to his photon, Bob can deterministcally recover the state Charles wanted to send.

2. IMPLEMENTING SUPERDENSE TELEPORTATION

Our system, shown in Fig. 1, creates time-bin and polarization hyperentangled pairs of photons via an unbalanced Mach-Zehnder interferometer[4] and type-0 spontaneous parametric downconversion in a polarizing Sagnac interferometer[5,6] with a periodically-poled lithium niobate crystal. Using a 532-nm mode-locked pump laser, we produce pairs of entangled photons at 1550 nm and 810 nm. The joint state of the system is of the form

$$|\psi\rangle = \frac{1}{2}(|(Ht_1)_{1550}(Ht_1)_{810}\rangle + |(Vt_1)_{1550}(Vt_1)_{810}\rangle + |(Ht_2)_{1550}(Ht_2)_{810}\rangle + |(Vt_2)_{1550}(Vt_2)_{810}\rangle). \quad (3)$$

Charles imparts his phases via liquid crystals in the horizontal/vertical basis. Alice measures in a mutually unbiased basis by using a polarizing beamsplitter in the diagonal/anti-diagonal basis (from the half-wave plates before the polarizing beamsplitter) and projecting onto superpositions of the time bins, using HWP3 and HWP4 after her unbalanced interferometer (see Fig. 1). Bob uses the components in his analyzer interferometer to perform a quantum state tomography for every photon incident on his detectors with a partner coincidentially detected on one of Alice's detectors within 1 ns.[7]

We have previously made measurements on the state fidelity of the transmitted states during SDT,[7–9] and attained an average fidelity of 0.94 ± 0.02 when measuring all combinations of ϕ_1, ϕ_2, and ϕ_3 at 45° intervals. See Ref. 7 for a more detailed analysis on the performance of SDT in this system.

3. ACTIVE SWITCHING FOR SDT

We use an unbalanced Mach-Zehnder interferometer (UMZI) to create and measure our time bins. After going through two UMZIs, there are 3 possible times a pulse can exit. The earliest (latest) time corresponds to the light taking the short (long) path in both UMZIs. If the light takes one short and one long arm, the final photon will be found in the middle time bin. This middle time is what we are interested in because it allows us to make measurements of time-bin superpositions and on individual time bins. Currently, we use a non-polarizing 50/50 beamsplitter at the entrance of Alice/Bob's measurement UMZI, which allows 50% of the light to exit at the long-long and short-short times. We are testing an active, polarization-independent switch,[9] in order to put 100% of the light into the middle time where we want to make our measurements.

Our testbed setup, shown in Fig. 2, involves sending a pulsed 785-nm laser through a series of beam displacers, waveplates, a Pockels Cell (PC), and a polarizing beamsplitter, collecting into single-mode fiber at the end. The laser and PC are driven at 100 kHz at 25% and 50% duty cycles for the laser and PC, respectively*

*In order to produce the signals for the laser and PC, a phase-locked loop is used on a field-programmable gate array (FPGA). The signal for the laser is directly connected to the 785-nm pigtail laser diode which is attached to a collimation package. The PC signal is sent from the FPGA through a comparator circuit and then another amplifier designed for the PC. The voltage applied to the PC is determined by the supply voltage for the comparator. Using the user manual for the PC, the comparator supply voltage is determined by $V_{-\pi/2}$ and $V_{\pi/2}$ along with the gain of the amplifier for the PC; these values are then tuned by direct measurement of the extinction ratios (discussed in more detail later).

The signals sent from the FPGA are phase-locked and adjusted to be at a relative phase such that the laser pulse is enveloped by the PC signal in time. A phase-locked loop (PLL) on the FPGA converts a 50-MHz clock into two 100-kHz signals with 25% and 50% duty cycles. The PLL is equipped with dynamic phase-shifting which allows the relative phase between the two signals to be adjusted while the signals are being sent so that the PC signal may envelop the laser pulse in time.

A comparator circuit using an open-loop, op-amp circuit is used to drive the PC signal from the FPGA. The comparator threshold is set at half the amplitude of the digital signals from the FPGA. The circuit uses potentiometers to allow tuning of the supply voltages to the op-amp. It also uses a rail-to-rail op-amp so the output of the circuit has peaks at the given supply voltages. The supply voltages are chosen so the PC is driven by a signal where the minima and maxima are $V_{-\pi/2}$ and $V_{\pi/2}$. Depending on whether the switch should be "on" or "off", the laser and PC are driven such that the laser pulse passes through the PC while the applied PC voltage is at its maximum or minimum. These maximum and minimum values are determined by the voltages at which the PC performs $-\pi/2$ and $\pi/2$ phase shifts, $V_{-\pi/2}$ and $V_{\pi/2}$.

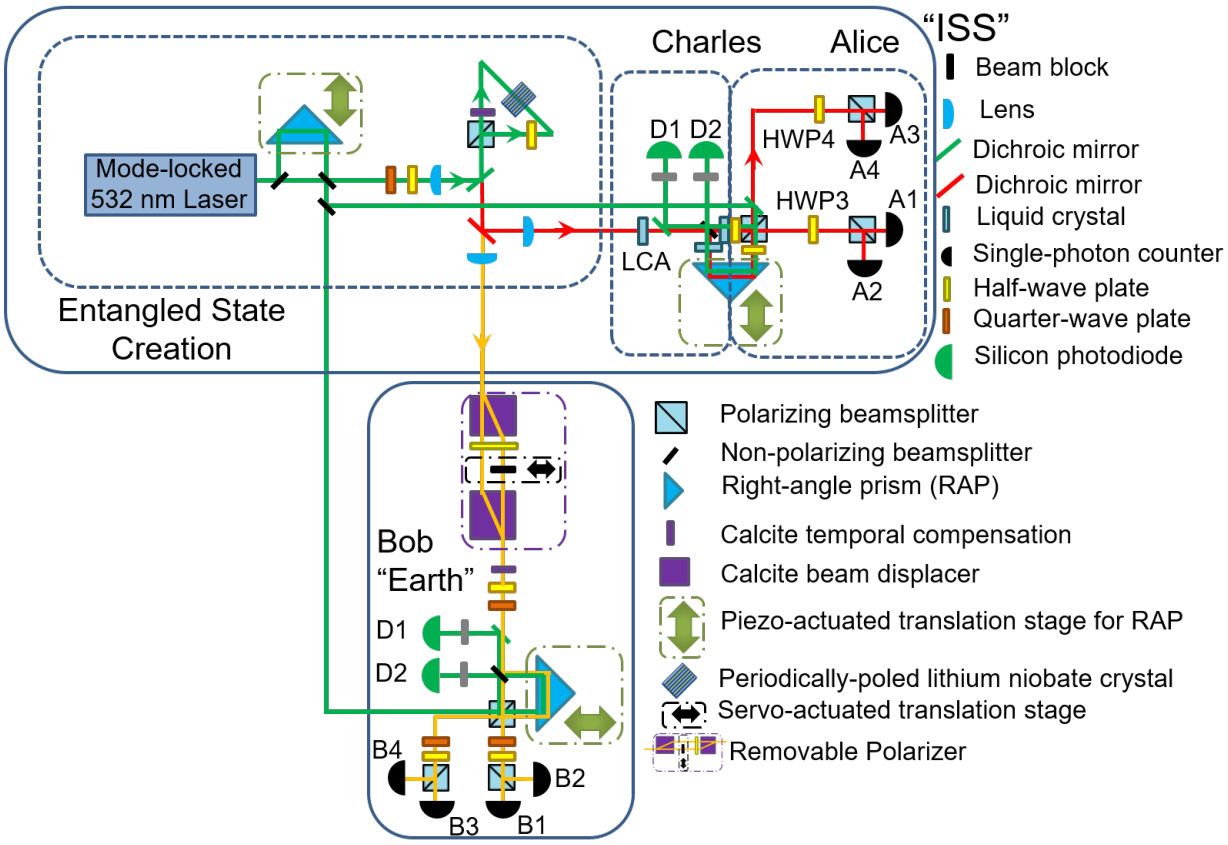

Figure 1: Using spontaneous parametric downconversion in periodically-poled lithium niobate and an unbalanced Mach-Zehnder interferometer we generate time-bin and polarization hyperentangled photon pairs. Green lines are the 532-nm pump (and stabilization) beam; red and yellow are the signal (810 nm) and idler (1550 nm) photons, respectively. Each half of the entangled state is manipulated and measured independently via Alice/Charles' and Bob's sections, which include polarization analysis, phase control, and an unbalanced interferometer for measurements of superpositions of time bins. LCB and HWP1 are inside the short path and LCC and HWP2 are inside the long path of Alice/Charles' delay interferometer.[7]

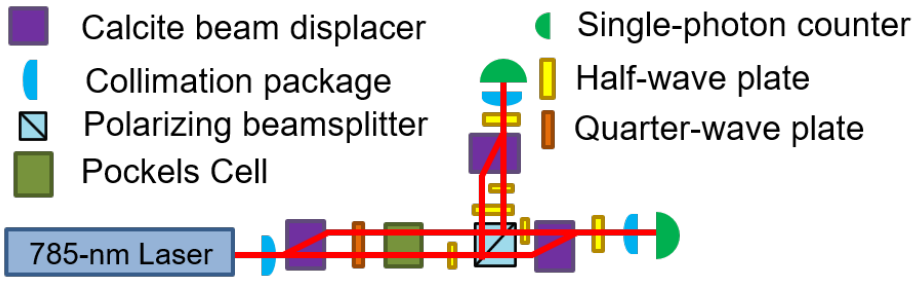

Figure 2: Polarization-independent active switch. Different polarizations are split into separate spatial modes and transmitted through a pockels cell which rotates the polarization of both beams accordingly; with a half waveplate in only one of the two arms, the polarizations are equal, so they are both transmitted or reflected at the polarizing beamsplitter. After the polarizing beamsplitter, the beams are recombined into a single spatial mode.

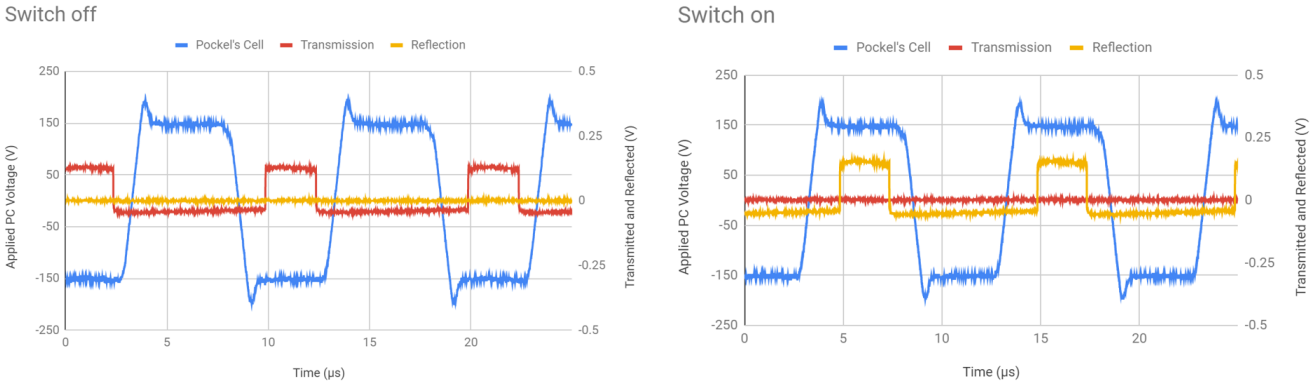

(a) (b)

Figure 3: (a) The blue Pockels cell monitor trace shows the instantaneous voltage applied to the PC. The red and yellow oscilloscope traces show the instantaneous power collected by the fast silicon photodiodes at the transmitted and reflected ports, respectively. The relative phase of the laser and PC voltage is such that the signal is always transmitted, corresponding to the "switch off" state. (b) The relative phase of the laser and PC voltage is such that the signal is always reflected, corresponding to the "switch on" state.

The beam propagates from a 785-nm fiber-pigtailed laser diode into a collimation package, and then into a calcite beam displacer. After going through a quarter-wave plate (QWP), the polarization of the beams are circular. The circularly polarized beams enter a pockels cell with its fast axis at 45° with respect to horizontal. A voltage on the pockels cell producing a $-\pi/2$ phase shift between horizontal and vertical polarization, $V_{-\pi/2}$, essentially cancels the effect of the QWP (assuming the QWP is rotated about its fast axis to ensure its applying exactly a $-\pi/2$ phase shift). Whereas, a voltage on the pockels cell producing $\pi/2$ phase shift between horizontal and vertical polarization, $V_{\pi/2}$, combines with the phase shift from the QWP to act like a half-wave plate (HWP) with its fast axis at 45° which rotates horizontal polarization to vertical and vice versa. One path goes through a HWP to make its polarization the same as the other path next to it. Both beams are transmitted (if $V_{PC} = V_{-\pi/2}$) or reflected (if $V_{PC} = V_{\pi/2}$) at the polarizing beamsplitter since they have the same polarization. The other half-wave plates rotate the polarization to ensure that both beams propagated the same distance upon recombination at the output beam displacers and that the overall transformation on the polarization is an identity and not an inversion in the H/V basis. The output beams are coupled into single-mode fibers using collimation packages. To measure the output, high speed silicon detectors measure the coupled beam and produce a voltage measured on an oscilloscope.

In Fig. 3a, we show that when $V_{-\pi/2}$ is applied to the PC before the laser pulse arrives and is held until after it leaves, the laser pulse is transmitted; this is the "switch off" state. Conversely, in Fig. 3b, when $V_{\pi/2}$ is applied to the PC, the laser pulse is reflected; this is the "switch on" state. The extinction ratio is 228:1 for the transmitted port of this optical switch and 160:1 for the reflected port. Since the PC has a QWP before it, we found it necessary to rotate the QWP about its fast axis to achieve maximum extinction. System efficiency measurements are currently underway.

We plan to measure a process tomography of the switch to further characterize its polarization independence. A burst mode will also need to be implemented. Currently the PC and laser are driven periodically, but we will need to change from the "switch on" and "switch off" states within the time-bin separation time ($\sim$ 1 ns). Finally, to realize the full improvement in efficiency we also would need to use a pockels cell that can operate at the same repetition rate as the pump laser. This is currently unavailable in free-space but a fiber-based modulator can easily achieve $\sim$100 MHz. Further investigation is needed to determine if this system could be implemented with all fiber-based components.

4. PASSIVE INTERFEROMETER PHASE STABILIZATION

Currently, we use active stabilization to hold the phase between $|t_1\rangle$ and $|t_2\rangle$ stable against environmental fluctuations. This involves two stabilization systems, one for the pump-Alice combined interferometer and another for the pump-Bob combined interferometer. We direct some of the 532-nm pump light that goes through the pump UMZI to each of the analyzer UMZIs. It goes in the reverse direction through Alice and Bob's UMZI as the quantum light and is in a different spatial mode, to reduce unwanted coupling in their single-photon detectors. In particular, the stabilization beam going through Alice's UMZI is vertically displaced so it does not go through the liquid crystals used for phase setting in the SDT protocol. The light is measured by two Si photodiodes at the output ports. Using a proportional-integral-derivative feedback mechanism and piezo-electric actuators, we adjust the position of the right angle prisms in the corresponding UMZI to maintain a stable relative phase.

In our notional experiment to deploy a hyperentangled pair source and implement SDT from space to earth, the entanglement source, Charles, and Alice would be in space and Bob would be at the receiving ground station on Earth. To avoid any moving parts in space, we want to passively stabilize the pump-Alice combined interferometer. Light Machinery, Inc. constructed an assembly which has Alice's UMZI vertically displaced from the pump UMZI but using the same optics; see Fig. 4. Since Bob's UMZI still needs to be stabilized with respect to the pump's, we designed the pump UMZI optics to function for 532 nm and 1540 nm. The 1540-nm stabilization beam can be co-transmitted to the ground with Bob's 1550-nm signal to stabilize the relative phase of the pump-Bob combined interferometer.

Our custom, stacked UMZI consists of two UMZIs, one positioned above the other. Each operates on the same optics, but there are different optical coatings for the top and bottom halves. There are two stacked, dual coated beamsplitter cubes and two dual-coated, 2" mirrors. The top level is coated for 810-nm light and the bottom for 532-nm and 1540-nm light. The 810-nm path has a liquid crystal controller in each arm to change the phase difference between the short and long paths. These components all sit within an INVAR metal case (INVAR is a 64-36% mix of iron and nickel), which has an exceptionally small thermal expansion coefficient. Fiber couplers are positioned at each port of the beamsplitter stacks for both interferometers.

Operation of the stacked UMZI requires that path-length differences of the 810-nm and 532-nm UMZIs are equal. If the path-length difference of the top and bottom change by the same amount at the same time, then there is no change in the relative phase. However, if the top and bottom UMZI path length differences change length differently, then operation is less than ideal. This is the motivation for dual coating the optics: If the optics or casing thermally expand or contract in some arbitrary way, there should not be any relative path-length difference changes between the 810-nm and 532-nm UMZIs since the top and bottom halves of the optical components cannot move relative to each other.

4.1 Interferometer Characterization

The first test is to verify that the 810-nm and 532-nm path-length differences are the same to within ~ 20 μm. 20 μm is chosen so that any path length difference will not affect the temporal entanglement visibility that has a coherence length ~ 500 μm. We measure path-length difference by constructing a separate reference UMZI, built on a translation stage in order to freely match the path length difference of the 532-nm and 810-nm UMZIs, and observe where the maximal visibility takes place for each. The 810-nm and 532-nm UMZIs are measured one at a time. We used a pulsed 810-nm laser (with coherence time ~ 350 fs) for the 810-nm UMZI measurement and a 532-nm pulsed laser (with coherence time ~ 7 ps) to measure the 532-nm UMZI. The peak visibility in the reference UMZI occurs where its path-length difference matches that of the UMZI being measured.

The beam which traverses the short arm of the 532-nm/810-nm UMZI and then the long arm of the reference UMZI (hence 'short-long path') interferes with the beam traversing the long arm of the 532-nm/810-nm UMZI and the short arm of the reference UMZI (hence 'long-short path'). The path-length difference of both the 810-nm and 532-nm UMZIs is ~ 1 ns. Since we used 810-nm and 532-nm lasers with coherence times much shorter than 1 ns, there was no interference within a single UMZI. Only the short-long and long-short paths interfere (when including the reference UMZI). The absolute visibility of these fringes is not important to characterize the path-length difference of each UMZI, only the adjusted path length of the reference UMZI needed to maximize

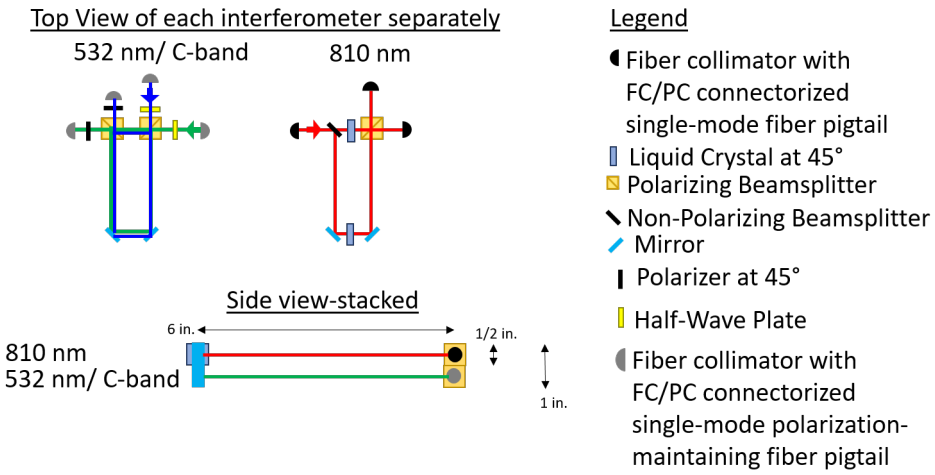

(a)

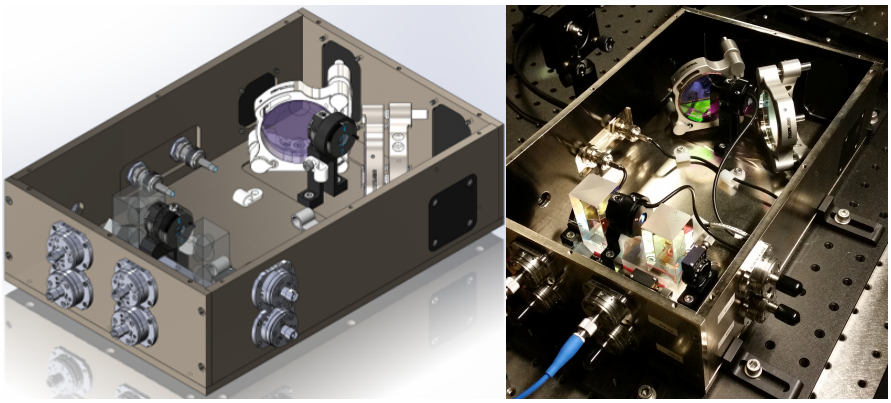

(b) (c)

Figure 4: (a) Functional diagram of stacked UMZI. All inputs and outputs are single-mode fiber coupled. Alice (810-nm) optics are on top with pump/stabilization (532-nm/1540-nm) below. (b) Design drawing of stacked UMZI designed. (c) Picture of stacked UMZI assembly constructed by Light Machinery, Inc.

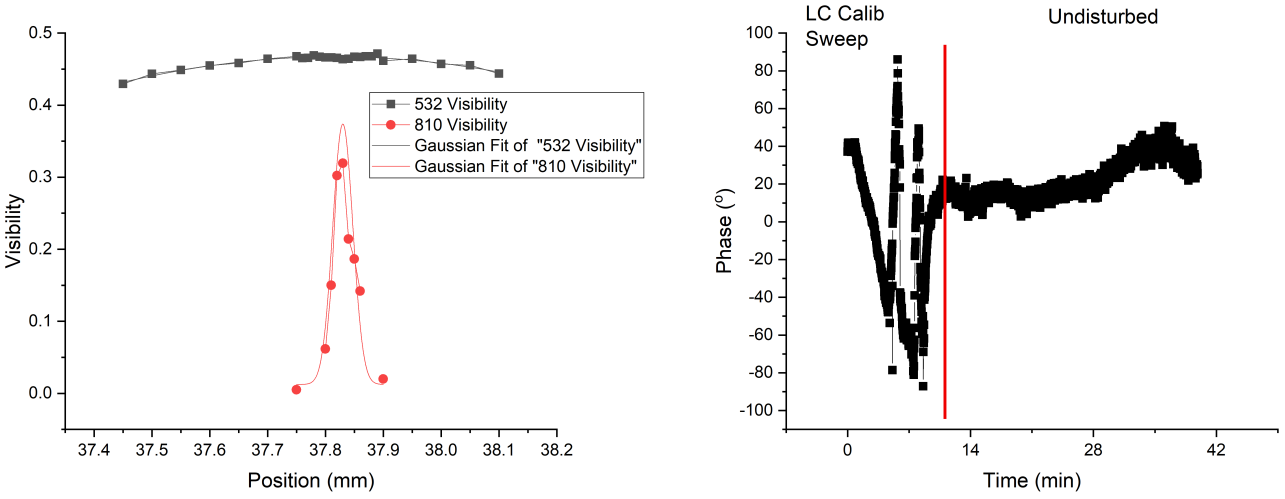

(a) (b)

Figure 5: (a) Visibility of 810-nm and 532-nm light when traversing their respective sections of the stacked UMZI interferometer and an external reference UMZI, plotted against the position of the external UMZI long-path micrometer. (b) Relative phase of long-short and short-long paths using a 690-nm laser and both sections of the stacked UMZI. The initial 11 minutes, the liquid crystal was actuated to sweep through several fringes. The remaining 30 minutes, the stacked UMZI was left, untouched and the liquid crystal was held constant.

it. We used a micrometer to finely tune the reference interferometer path length and plotted the results using a piezo-electric actuator to vary the phase for the visibility measurement. In Fig. 5a, we plot the measured visibility as a function of the reference UMZI long-arm micrometer position for both the 532-nm and 810-nm UMZIs. We fit each curve to a Gaussian and calculate the difference between the peak position for 532 nm and 810 nm is 26 ± 2 μm.

To test the passive stability of the relative path-length differences of the 810-nm and 532-nm sections, we measured the phase between the 532-nm long path + 810-nm short path and the 532-nm short path + 810-nm long paths, using a single-mode fiber to connect the output of the 532-nm UMZI to the input of the 810-nm UMZI. The optical coatings on the long-path mirrors do not overlap much in their high-reflectivity regimes. We improvised with a 690-nm continuous wave (CW) diode laser, although the loss from coupling inefficiencies (the fiber couplers have improper focal lengths for 690-nm beams) and poor transmission amounts to 99.99%. We adjusted the fiber couplers and polarization fiber controllers on the single-mode fiber linking the 810-nm and 532-nm UMZIs to obtain interference between the short-long and long-short paths. Using the liquid crystals to manually sweep the phase of the 810-nm long arm, we were able to scan the entire range of interference fringes. This appears on Fig. 5b as several sharp peaks at the start of the test. This allows us to calibrate phase vs optical power for an output port, assuming the laser power is held constant.

The liquid crystals remained set to one phase, and the setup was left untouched in an empty, temperature-controlled lab space for half an hour. The phase variation over time is recorded in Fig. 5b. In the ideal case, the time interval would show no phase change; however, the setup appears to slowly pass through a 30° phase shift but that may not be due to the relative path-length differences of the 810-nm and 532-nm sections. The 690-nm CW has a coherence length time than 1 ns so it interferes with itself within a single UMZI, which we do expect to have appreciable phase drifts. Additionally, this measurement did not employ normalization of the input optical power. We plan to implement normalization and we are in the process of setting up a pulsed 690-nm laser with a short enough coherence time to isolate the stability of the relative path-length differences of the 810-nm and 532-nm sections. Once the stability of the relative path-length differences of the 810-nm and 532-nm sections is measured, we will proceed with heating the INVAR case in various ways to see what the system can tolerate.

4.2 Future Temperature Sensitivity Characterization

This stacked UMZI setup is meant to influence the design of a model which will go on the ISS. The Station's exposure requires equipment to withstand temperature variations from $-20°C$ to $70°C$. Either the UMZI must tolerate these variations, or we must control the environment to remove them. The first test is to observe the stability of the relative path-length difference between the 810-nm and 532-nm UMZIs as a function of time. Once we know it is stable, we can vary the temperature manually to see what the stacked UMZI can tolerate, and if we need further insulation or active temperature control.

We want to heat our interferometer in areas that may affect the pathlength difference, e.g., below the beam-splitters, in the middle of the long path of the laser and by the mirrors. We will use a 3-Ohm, 50-W Resistor and 12-V, 5-A DC power supply connected in series, achieving a maximum power of 48 W. The resistor acts as a heater because of the power it dissipates; it can heat itself up from $20°C$ to $70°C$ in just a few minutes. To have a slower increase in temperature and to hold the temperature constant at a specific temperature, we will explore several options. The first option is to lower the voltage across the resistor, to reduce the heat dissipation which will slow the increase in temperature. The second option is to use pulse-width modulation and proportional integral derivative (PID) code running on the microcontroller to keep the temperature at a specific setpoint. Given that we are currently observing rapid increases in temperature, using both options might prove most effective.

Once we have characterized the interferometer performance using our resistor heater setup, we will move to cooling the interferometer as we want to characterize operation from $-20°C$ to $> 70°C$, to reach the full operating temperature range experienced on the ISS. Using a similar setup as the heater, we can position a Peltier thermoelectric cooler[10] in a square area anywhere on our interferometer to cool it to our desired temperature, $-20°C$.

In order to use more than one sensor to measure the temperatures within the interferometer, we will use an I^2C-multiplexer to change the I^2C-addresses of our sensors so they can be detectable and differentiable from one another. By doing this, we can have up to 8 different temperature sensors set up on our interferometer to measure how our targeted temperature heating (and cooling) changes the temperature of specific parts of the interferometer. We can therefore have sensors at the liquid crystal, near the input and output lasers and by the mirrors. This will allow us to determine which part or parts of the interferometer, when heated, have the most significant impact on the relative path-length difference.

5. CONCLUSION

Here we have explored several methods to improve our system that implements SDT. To increase the efficiency of SDT by a factor of 2, we have begun characterization of an active optical switch to be placed in Alice's analyzer interferometer. The measured switching extinction ratios look promising but further characterization is necessary to completely assess the viability of this possible system improvement. With the goal of passive stabilization, Light Machinery, Inc. constructed a tri-wavelength, stacked unbalanced Mach-Zehnder interferometer and we have begun characterization of it. The path lengths of the stacked UMZIs are sufficiently matched. The stability of this system has been bounded to less than $30°$ drifts. Further characterization is needed to measure the phase stability of the stacked UMZI without artifacts from power drifts and interference in a single UMZI.

ACKNOWLEDGMENTS

This work was primarily supported by NASA Grant No. NNX16AM26G. This work was also supported by a DoD, Office of Naval Research, National Defense Science and Engineering Graduate Fellowship (NDSEG).

REFERENCES

[1] Hughes, R. J. et al., "Quantum cryptography for secure satellite communications," *IEEE Aerospace Conf. Proc.* (2000).

[2] Aspelmeyer, M., Jennewein, T., Pfennigbauer, M., Leeb, W. R., and Zeilinger, A., "Long-distance quantum communication with entangled photons using satellites," *IEEE J. of Sel. Top. in Q. Elec.* **9**(6), 1541–1551 (2003).

[3] Bernstein, H., "Superdense quantum teleportation," *Quant. Info. Process.* **5**, 451–461 (2006).
[4] Marcikic, I. et al., "Time-bin entangled qubits for quantum communication created by femtosecond pulses," *Phys. Rev. A* **66**(6), 062308 (2002).
[5] Shi, B. S. and Tomita, A., "Generation of a pulsed polarization entangled photon pair using a sagnac interferometer," *Phys. Rev. A* **69**(1), 013803 (2004).
[6] Kim, T., Fiorentino, M., and Wong, F. N., "Phase-stable source of polarization-entangled photons using a polarization sagnac interferometer.," *Phys. Rev. A* **73**(1), 012316 (2006).
[7] Chapman, J. C., Graham, T. M., Zeitler, C. K., and Kwiat, P. G., "Time-bin and polarization superdense teleportation for space applications," *arXiv preprint* (arXiv:1901.07181) (2019).
[8] Chapman, J. C., Bernstein, H., Meier, K., Zeitler, C., and Kwiat, P. G., "Progress towards implementing superdense teleportation in space," *Proc. SPIE* **10547**, 105470 – 105478 (2018).
[9] Graham, T. M., *Using Hyperentanglement for advanced quantum communication*, PhD thesis, University of Illinois at Urbana-Champaign (2016).
[10] Peltier, J.-C., "Nouvelles expériences sur la caloricité des courants électrique," *Ann. Chim. Phys* **56**(371), 371–386 (1834).